International Journal of Pharmaceutics 651 (2024) 123754

Contents lists available at ScienceDirect

International Journal of Pharmaceutics

journal homepage: www.elsevier.com/locate/ijpharm

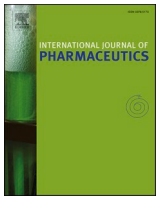

Nanocrystal-chitosan particles for intra-articular delivery of disease-modifying osteoarthritis drugs

Luca Morici [a,b,1], Paula Gonzalez-Fernandez [a,b,1], Sébastien Jenni [a,b], Alexandre Porcello [a,b], Eric Allémann [a,b], Olivier Jordan [a,b,*], Carlos Rodríguez-Nogales [a,b,*]

[a] School of Pharmaceutical Sciences, University of Geneva, Rue Michel-Servet 1, 1211 Geneva 4, Switzerland
[b] Institute of Pharmaceutical Sciences of Western Switzerland, Rue Michel-Servet 1, 1211 Geneva 4, Switzerland

ARTICLE INFO

Keywords:
Osteoarthritis
Intra-articular
Nanocrystals
Spray drying
Chitosan
Kartogenin

ABSTRACT

Osteoarthritis is the most common chronic joint disease and a major health care concern due to the lack of efficient treatments. This is mainly related to the local and degenerative nature of this disease. Kartogenin was recently reported as a disease-modifying osteoarthritis drug that promotes cartilage repair, but its therapeutic effect is impeded by its very low solubility. Therefore, we designed a unique nanocrystal-chitosan particle intra-articular delivery system for osteoarthritis treatment that merges the following formulation techniques: nanosize reduction of a drug by wet milling and spray drying. The intermediate formulation (kartogenin nanocrystals) increased the solubility and dissolution rates of kartogenin. The final drug delivery system consisted of an easily resuspendable and ready-to-use microsphere powder for intra-articular injection. Positively charged chitosan microspheres with a median size of approximately 10 μm acted as a mothership drug delivery system for kartogenin nanocrystals in a simulated intra-articular injection. The microspheres showed suitable stability and a controlled release profile in synovial fluid and were nontoxic in human synoviocytes. The cartilage retention skills of the microspheres were also explored *ex vivo* using cartilage. This drug delivery system shows promise for advancement to preclinical stages in osteoarthritis therapy and scale-up production.

1. Introduction

Osteoarthritis (OA) is the most common degenerative joint disease worldwide, with approximately 7 % of cases globally, and is associated with an extremely high economic burden each year (Leifer et al., 2022). OA physiopathology is complex and characterized by progressive cartilage degradation as well as activation of inflammatory pathways in the synovial membrane, chronic pain, subchondral bone remodeling and osteophyte formation. The only treatment options available are symptomatic and/or not effective due to the absent vascularization of the cartilage and the local and degenerative nature of this disease (Evans et al., 2014). In this context, disease-modifying OA drugs (DMOADs) are gaining interest in the field because they are potential modulators of disease progression. The small molecule kartogenin (KGN) is considered a DMOAD because it promotes the differentiation of human mesenchymal stem cells into chondrocytes and stimulates cartilage regeneration via the CBFβ-RUNX1 activation pathway (Marini et al., 2012). However, the therapeutic success of KGN is majorly impeded by its very low solubility, which has hampered its clinical options. Meanwhile, intra-articular (IA) drug injections remain unfulfilled due to fast clearance from the joint space (Evans et al., 2014; Maudens et al., 2018a).

Research on IA drug delivery strategies (*e.g.,* hydrogels, microparticles, or nanoparticles) is progressively gaining relevance in OA management. However, no hydrogels for drug delivery are currently commercially available, with the exception of hyaluronic acid gels for viscosupplementation (Gonzalez-Fernandez et al., 2022; Maudens et al., 2018a). Polymeric microparticulate drug delivery systems have attracted increasing interest in the field, as a triamcinolone polymeric microsphere formulation has been marketed for IA injection in OA (Zilretta®) (Paik et al., 2019). Through these systems, high drug loadings can be achieved along with sustained drug release directly into the joint. To date, these approaches also entailed the formulation of several KGN biomaterials at the nanoscale and macroscopic level (Chen and Liao, 2023). Nevertheless, no KGN or other DMOADs have reached the

* Corresponding authors at: School of Pharmaceutical Sciences, University of Geneva, Rue Michel-Servet 1, 1211 Geneva, Switzerland.
E-mail addresses: Olivier.jordan@unige.ch (O. Jordan), Carlos.Rodriguez-Nogales@unige.ch (C. Rodríguez-Nogales).
[1] Contributed equally.

https://doi.org/10.1016/j.ijpharm.2023.123754
Received 23 October 2023; Received in revised form 27 December 2023; Accepted 28 December 2023
Available online 30 December 2023

market. Another major challenge is to attain cartilage targeting or retention with second-generation drug delivery systems once in the IA compartment (Bajpayee and Grodzinsky, 2017). While it remains to be fully explored, this approach is expected to significantly boost the therapeutic perspectives of DMOADs in the clinic.

In this study, we designed a unique KGN delivery system for IA administration in OA. This approach combines the following formulation techniques: nanosize reduction of the active ingredient by wet milling and subsequent spray drying to form chitosan (CH) microspheres (MPs) loaded with KGN nanocrystals (NCs). Wet milling is a common top-down methodology to produce drug NCs that provides a second opportunity for poorly soluble drugs (Malamatari et al., 2018). The small size of the wet milled suspension is also crucial to for the effective and homogeneous incorporation/redispersion in the spray dryer feed solution. Spray drying is a scalable technique that converts a liquid into a dried powder when atomized droplets pass through a heated gaseous medium (Sosnik and Seremeta, 2015). This technique is a time/cost-saving process largely used for pharmaceuticals and biopharmaceuticals (Ziaee et al., 2018). CH is a natural biodegradable and biocompatible cationic linear hydrophilic polysaccharide composed of residues of glucosamine and N-acetyl-glucosamine produced by chemical deacetylation of chitin from crustacean sources (Kantak and Bharate, 2022). In an aqueous acidic medium, the solubility of CH increases via protonation of the primary amines, and this has allowed for the development of many kinds of delivery systems for multiple drugs up to this date (Aranaz et al., 2021; Vårum et al., 1994). These singularities also encouraged us to spray-dry this polymer to obtain cationic MPs that can load KGN NCs for the first time. While displaying suitable biocompatibility, CH MPs may also adequately stabilize KGN NCs and ameliorate their release profile in the IA environment (Emans et al., 2023). In addition, the cationic strength of these MPs is also expected to interact with negatively charged cartilage, improving the retention and drug release of KGN at the site of action (Warren et al., 2022).

In this work, we described the development process and characterization of KGN NCs loaded into MPs for the treatment of OA. First, KGN was successfully synthesized and recrystallized, and then, the drug was wet-milled in the presence of a stabilizer. To obtain an MP dry powder, the aqueous KGN nanosuspension was then directly incorporated into a spray drying feed solution containing CH. The physico-chemical properties of the two formulations were characterized, and their aptitudes as IA drug delivery systems were compared. To mimic IA administration, *in vitro* toxicity was tested in primary synoviocytes, and their stability and drug release behavior were evaluated directly in horse synovial fluid (SF). Finally, an *ex vivo* bovine cartilage set up was designed to investigate the electrostatic interaction between the negative fixed charge density of the cartilage and the positive surface charged CH MPs.

2. Experimental section

2.1. Materials

Ethanol and tetrahydrofuran were acquired from Fisher Scientific (Waltham, MA, USA). Phthalic anhydride was purchased from Acros Organics (Geel, Belgium), ethyl acetate, glutaraldehyde, dimethylsulfoxide, D-α-Tocopherol polyethylene glycol 1000 succinate, acetonitrile (analytical grade), phosphate buffer saline tablets, polyvinylpyrrolidone (MW 40,000), kartogenin (commercial), 4-aminobiphenyl, low (50–190 kDa), medium (190–310 kDa) and high (310–375 kDa) MW 75–85 % deacetylated chitosan, sterile phosphate buffer saline (PBS), RPMI-1640 and M199 cell media were supplied by Sigma-Aldrich (Sant Louis, MO, USA). Formic acid was acquired from Reactolab SA (Servion, Switzerland). Yttrium-stabilized zirconium oxide (ZrO_2) Ø 0.5-mm grinding beads were purchased from Next Advance (Troy, NY, USA). WST-1 cell proliferation assay was purchased from Roche Applied Science (Basel, Switzerland). Fetal bovine serum was purchased from Eurobio (Les Ulis, France). Trypsin-EDTA and penicillin/streptomycin were provided by Gibco® (Invitrogen Inc., Carlsbad, USA). Equine synovial fluid was aspirated from six fetlock joints, obtained after slaughter from healthy adult horses (Communal slaughterhouse, Delémont, Switzerland) and stored at −80 °C. Fresh bovine knee joint cartilage was donated from a local butcher shop (Boucherie Chevaline du Vieux Carouge, Geneva, Switzerland).

2.2. Synthesis and recrystallization of kartogenin

4-Aminobiphenyl (1 g, 5.91 mmol, 1 eq) and phthalic anhydride (0.963 g, 6.50 mmol, 1.1 eq) were dissolved in ethyl acetate (100 mL). The solution was stirred at room temperature for 2 h, and a white precipitate was formed. The reaction mixture was filtered under vacuum, and the precipitate was washed with ethyl acetate. Finally, the solid was recrystallized using tetrahydrofuran (50 mL) and water (50 mL) and dried under high vacuum to obtain a white powder (1.47 g, 78 % yield). ^{1}H NMR (600 MHz, DMSO-d_6) δ 13.05 (s, 1H), 10.44 (s, 1H), 7.88 (d, 1H), 7.81–7.76 (m, 2H), 7.69–7.62 (m, 5H), 7.61–7.55 (m, 2H), 7.48–7.42 (m, 2H), 7.36–7.30 (m, 1H). ^{13}C NMR (151 MHz, DMSO-d_6) δ 167.92, 167.89, 140.27, 139.54, 139.33, 135.45, 132.21, 130.43, 130.03, 129.90, 129.38, 128.28, 127.49, 127.31, 126.75, 120.30. LRMS ESI-: *m/z* 316.0 $[M-H]^-$ calculated for $C_{20}H_{14}NO_3$ 316.1 (see SM for further information).

2.3. Formulation of kartogenin nanocrystals

Size reduction of recrystallized KGN was performed using a homogenizer (Precellys 24®) from Bertin Instruments (Montigny-leBretonneux, France). 25 mg of the drug were added to a 2-mL tube with the stabilizer D-α-Tocopherol polyethylene glycol 1000 succinate (TPGS) or polyvinylpyrrolidone (PVP) at the drug-to-stabilizer w/w ratio 1/0.1. Lastly, 600 mg of zirconium oxide 0.5-mm beads and 1 mL of Milli-Q water were added to each tube. The complete sequence was ten cycles of 90 s at 8,400 rpm followed by five cycles of 15 s at 10,000 rpm and finally ten cycles of 70 s at 6,600 rpm. Aqueous nanosuspensions were stored at 2–8 °C until further characterization.

2.4. Spray drying of chitosan microspheres

CH MPs were formulated using a 4 M8-TriX semi-industrial spray dryer (ProCepT, Zele, Belgium). Briefly, low-, medium-, or high-MW CH (1 % w/v) with or without KGN NCs at a theoretical drug loading of 16 % w/w was dissolved in 10 mL of a water:ethanol (9:1 v/v) mixture acidified with formic acid (1 % v/v) under continuous agitation at 50 °C. Crosslinking of CH was performed by the addition of glutaraldehyde (GA) to the feed solution at different ratios (0–2.5 % v/v) for 60 s. Dried MPs were stored at 2–8 °C for further characterization. After optimizations, the following process parameters were fixed: low MW CH concentration 1 % w/v; GA concentration 1 % v/v; feed solution rate 5 mL/min; bi-fluid nozzle 0.6 mm (internal diameter); atomizing air force 10 mL/min; inlet temperature 90 °C; outlet temperature 57 °C; cyclone size small and inlet air flow 0.28 m^3/min. Air was chosen as the processing gas.

2.5. Particle characterization

Particle size distribution (PSD) was determined using a Mastersizer 3000 (Malvern, Worcestershire, UK) laser diffraction equipment. Aqueous nanosuspensions (KGN NCs) were measured directly, whereas spray dried MPs were redispersed in a 0.1 % w/v TPGS aqueous solution prior to measurements. The particle size measurements were expressed as the volume diameter (Dv) using'Mastersizer v3.60.' software (Malvern, Worcestershire, UK). The refractive index used was 1.59 for the particles and 1.33 for the dispersant (Milli-Q water).

The zeta potential of MPs and NCs was measured at 25 °C using a Zetasizer Nano ZS Malvern (Malvern Instruments SA, Worcestershire,

UK) after the samples were diluted in Milli-Q water in a folded capillary cell and using the Smoluchowski equation.

Particle morphology was visualized using a JSM-7001F emission scanning electron microscope (SEM) (JEOL, Tokyo, Japan). For NCs, one drop of the suspension was placed after dilution in a glass holder and evaporated under vacuum. Spray dried MPs were directly deposited onto carbon tape-covered metal studs. Prior to analysis, the studs were sputter-coated with gold (20 nm thickness) with a Leica EM SCD005 (Leica Microsystems, Germany) for approximately 44 s at 40 mA. All micrographs were acquired at a 5 kV voltage for MPs and 15 kV for NCs.

Characterizations of the formulations in SF (previously filtered using 0.45 μm disposable syringe filters) were performed after 1 h incubation at 37 °C in an orbital shaker at 100 rpm. For PSD analysis, the suspensions were directly introduced into the laser diffraction chamber. For zeta potential and SEM analysis, suspensions were previously washed once with Milli-Q water.

2.6. Drug quantification by ultra high-performance liquid chromatography

Drug quantification was performed using an Acquity™ Ultra-performance LC (UHPLC) coupled to a photodiode array (PDA) detector (Waters Corp, Milford, MA, USA). Samples were separated using an Acquity UPLC® BEH C18 column (2.1 mm × 50 mm, 1.7 μm, Waters, USA) coupled to a C18 1.7 μm 2.1x 5 mm VanGuard™ pre-column (Acquity UPLC®) equilibrated at 40 °C. A 2-min gradient elution at a constant flow rate of 0.4 mL/min was performed using a mobile phase composed of 50 to 10 % of a 0.05 % (v/v) formic acid aqueous solution and 50 % to 90 % of 0.05 % (v/v) formic acid acetonitrile (ACN). Sample volume injection was 5 μL, and wavelength PDA detection was set at 280 nm. Representative peak chromatograms can be seen in Fig. S4AB.

The UHPLC methodology described above was used to quantify the drug content of all microparticulate systems and to calculate formulation yields of KGN NCs after wet milling. KGN was extracted from 2 mg of MPs vortexed/mixed with 250 μL of water formic acid 1 % v/v and 750 μL of dimethylsulfoxide (DMSO). For KGN extraction from SF, 10 μL of the sample was mixed with 90 μL of water formic acid 1 % v/v and 900 μL of ACN. Samples were vortexed/mixed for 2 min and centrifuged for 5 min at 10,000 rpm. With this setup, KGN recoveries in SF were above 90 %. The lower limit of quantification values were determined according to a signal/noise ratio > 10 and linearity $R^2 > 0.990$, obtained in independent experiments. Thus, calibration curves ranged from 0.1 to 15 μg/mL (Fig. S4C) and from 0.2 to 7.5 μg/mL for the SF samples (Fig. S4D).

2.7. Solubility and in vitro dissolution tests on kartogenin nanocrystals

Solubility studies were performed in tubes at a drug concentration of 2 mg/mL in Milli-Q water, PBS (pH 7.2–7.4) and horse SF. The suspensions were placed in an orbital shaker at 100 rpm at 37 °C, and the samples in Milli-Q water were incubated at room temperature (20 ± 1 °C). After 24 h of incubation, each tube was centrifuged at 10,000 rpm for 15 min. Recovered supernatants were then filtered using 0.20 μm disposable syringe filters and quantified using the above-described methods.

In vitro nanocrystals dissolution studies were performed in "sink" conditions over 24 h in PBS (pH 7.2–7.4) using Costar Transwell® permeable supports placed in an orbital shaker at 100 rpm at 37 °C. At allotted time points (15 min, 2, 4 and 24 h), the sample solutions in the lower compartments were quantified using the above-described methods.

2.8. Drug release studies

In vitro drug release studies of KGN CH MPs and KGN NCs were performed in both PBS and horse SF under saturation conditions. Tubes were capped to prevent water from evaporating and placed in an orbital shaker at 100 rpm at 37 °C. At allotted time points (2, 24, 72, and 120 h), each tube was centrifuged at 10,000 rpm for 15 min. Recovered supernatants were then filtered using disposable syringe filters (0.20 μm) and quantified using the above-described methodology. At the time points 24 and 72 h, the withdrawn supernatants were replaced with fresh release medium.

2.9. Cell culture and cytotoxicity assays

Human fibroblast-like synoviocytes (HFLS) from hip synovial OA patients (CCER, Geneva, Switzerland, authorization number 2017–02234) (Salgado et al., 2020) were maintained in RPMI 1640: M199 (1:1) cell medium supplemented with 10 % fetal bovine serum and 1 % penicillin/streptomycin. Cell culture flasks were placed in an incubator at 37 °C with a humidified atmosphere and 5 % carbon dioxide. Cellular experiments were performed from passage 3 until 9.

For the *in vitro* cytotoxicity assays, HFLS cells were seeded on 96-well plates at a density of 8,000 cells per 100 μL/well, 24 h before the addition of cell medium dilutions of commercial KGN (previously diluted DMSO resulting in a final concentration in cell medium of 1 % v/v), KGN NCs, CH MPs and KGN CH MPs in triplicate wells. After 72 h of incubation, the treatment medium of each well was replaced with complete cell medium containing the cell proliferation reagent WST-1. Absorbance was measured 3 h later in a microplate reader (Synergy Mx microplate reader, BioTek Inc., USA) at a test wavelength of 450 nm and 690 nm for the reference wavelength.

2.10. Ex vivo cartilage experiments

Bovine cartilage sections of 0.1x0.8x0.6 cm, previously washed with PBS, were incubated with the KGN NCs or KGN CH MPs in the presence of PBS or SF. The final KGN concentration was 1 mg/mL, and the total volume was 400 μL. After 5 min or 1 h incubation at 37 °C in an orbital shaker at 100 rpm, cartilage sections were withdrawn and immersed in Milli-Q water for 30 s. For KGN recovery, cartilage was incubated with 1 mL of ACN for 10 mins. KGN in the ACN solution was then quantified using the above-described methodology. Other cartilage sections were dried under vacuum and visualized by SEM to observe the presence of MPs on the surface.

2.11. Statistical analysis

Statistical comparison between different groups was performed using an unpaired *t*-test or ANOVA One-Way analysis (Tukey's multiple comparison test) with GraphPad Prism 8.0.1 software (San Diego, CA, USA). Data were reported as the mean ± s.d., considering a 95 % confidence interval at significance level * $p < 0.05$.

3. Results

3.1. Synthetized/recrystallized kartogenin was effectively wet milled

At the outset of the study, the one-step covalent coupling of 4-aminobiphenyl to phthalic anhydride was explored, leading to the precipitation of KGN in ethyl acetate (Fig. 1A). The obtained product was recovered with a yield of 78 % and characterized by ^{1}H NMR (Fig. S1A), ^{13}C NMR (Fig. S1B), and mass spectrometry (Fig. S2A). KGN was then recrystallized in a water/tetrahydrofuran mixture to improve size reduction of the starting material in subsequent steps. For instance, a fast recrystallization was prevented (Fig. 1B) in favor of a slow recrystallization obtained with equivalent volumes of tetrahydrofuran and water overnight. The product obtained presented larger and thicker crystal plates (Fig. 1C) and was suitable for wet milling.

Particle reduction to nanoscale size by wet milling was achieved only in the presence of nonionic surfactants or stabilizers (*e.g.,* TPGS at a

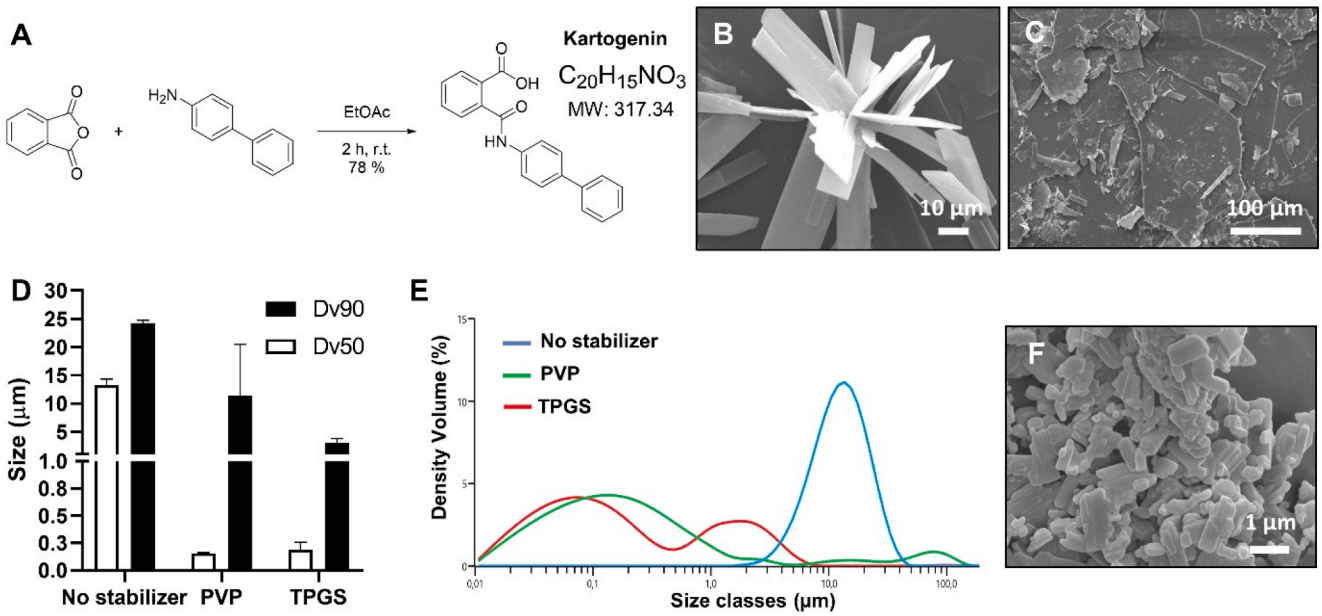

Fig. 1. (A) Schematic representation of the synthesis of KGN. SEM representative micrographs of fast KGN recrystallization (B) *vs.* slow KGN recrystallization (C). (D) PSD Dv50 and Dv90 values assessed by laser diffraction of wet milled slow recrystallized KGN using different stabilizers. (E) PSD representative graphs by volume density obtained by laser diffraction of wet milled slow recrystallized KGN using different stabilizers. (F) SEM representative micrographs of washed and lyophilized TPGS-stabilized KGN NCs.

KGN/stabilizer ratio 1/0.1). Under these conditions, a milky white suspension with no sedimentation events was observed. As seen in Fig. 1D, PSD Dv50 values were below 0.3 µm only with TPGS or PVP, another stabilizer used as control. Without stabilizer, reported Dv50 values for wet milled KGN were above 10 µm (Fig. 1D). In this case, the particles exhibited a unimodal distribution in the micron size range, as shown in the laser diffraction PSD graphs in Fig. 1E. In contrast, PSD curves were mostly below the size class threshold of 2–3 µm when TPGS or PVP were added to the formulation. SEM micrographs also confirmed the particle size reduction of KGN from the starting material (Fig. 1C). TPGS-stabilized KGN NCs in Fig. 1F displayed a population of four-sided polygonal or irregular particles below 1–2 µm in agreement with laser diffraction (Dv90 value was around 3.0 µm).

3.2. Nanocrystals improved the solubility and dissolution rates of kartogenin

Solubility tests of KGN NCs were performed under different conditions. In Milli-Q water, recrystallized KGN and commercial KGN, used as control, showed concentrations in solution of approximately 0.001 and 0.002 mg/mL, respectively (Fig. 2A). In the case of KGN NCs, these values were significantly increased by 2–3-fold. In PBS (pH 7.2–7.4) at 37 °C, KGN concentrations in solution drastically augmented up to 0.61–0.82 mg/mL, although no significant differences were found between the samples. Solubility was tested in horse SF at 37 °C as well. Concentrations in solution measured here were further increased up to 1.1–1.4 mg/mL. KGN NCs presented a wide standard deviation, but no significant differences were found among the tests. With that in mind, drug dissolution tests were performed over 24 h in PBS. A significant dissolution rate enhancing effect was observed for the NCs. After 2 h, a cumulative release plateau around 100 % was reached, while the

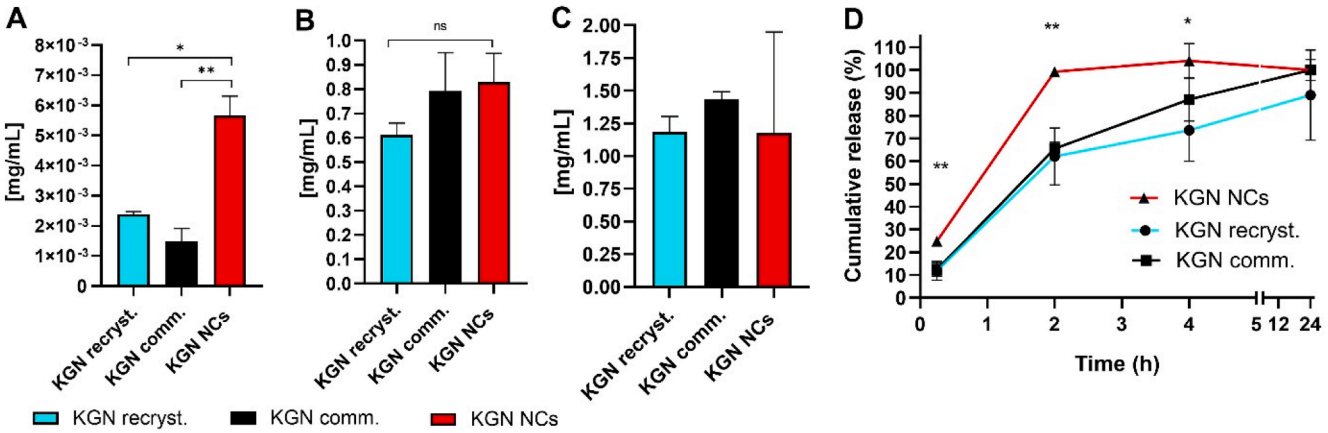

Fig. 2. Solubility tests of KGN NCs (red), recrystallized (light blue) and commercial KGN (black) were performed in (A) Milli-Q water at 20 ± 1 °C (pH 6–7), (B) PBS at 37 °C (pH 7.2–7-4) and (C) horse SF at 37 °C. (D) Dissolution profile of KGN NCs (red), recrystallized (light blue) and commercial KGN (black) in "sink" conditions in PBS at 37 °C. KGN was quantified by UHPLC. All results are represented by the mean ± sd ($n \geq 3$). * $p < 0.05$, ** $p < 0.01$; ns means non-significant. (For interpretation of the references to colour in this figure legend, the reader is referred to the web version of this article.)

percentages for the recrystallized and commercial KGN were still approximately 60 % of the total.

3.3. Formulation of kartogenin chitosan microspheres through spray drying optimizations

With the proposed technology approach, fresh aqueous nano-suspensions of KGN (*i.e.,* KGN NCs) were immediately incorporated in the spray drying feed solution together with CH. After some spray drying pre-optimizations, we simultaneously screened appropriate CH cross-linking and CH MW by mainly evaluating their PSD and/or resuspendability. The results obtained using CH with three different MWs showed that increasing amounts of GA correlated with reduced Dv50 and Dv90 values and/or better resuspension, as shown in Fig. 3A. Although MPs were apparently correctly formed (Fig. S5A), MP resuspension failed without crosslinking. Therefore, a GA concentration of 1 % v/v was set for the next experiments, as Dv50 and Dv90 values (15.2 ± 4 and 37.1 ± 9 μm, respectively) showed suitable particle size and/or resuspension. At that GA ratio, low MW CH displayed better trends with regards to particle size/resuspendability (*e.g.,* Dv90 < 40 μm) and reproducibility (yields > 30 %) in comparison with medium (Fig. S5B) and high CH MWs (Fig. S5C); therefore, low MW CH was also fixed for the final setup.

Several batches of blank and KGN CH MPs were formulated with the final parameter setup listed in the Experimental Section. Yields of 33.3 ± 5.5 % were achieved for blank CH MPs, and their PSD Dv50 and Dv90 values were 9.5 ± 4.0 and 29.6 ± 11.5 μm, respectively. For the loaded MPs, obtained yields were 33.5 ± 3.8 %, and Dv50 and Dv90 values were 11.2 ± 2.5 and 42.3 ± 9.1 μm, respectively. Laser diffraction PSD curves in Fig. 3C showed that the incorporation of KGN NCs in the formulation slightly increased the particle size observed for blank CH MPs. The efficacy of encapsulation was 70.3 ± 4.0 %, translating into a drug loading of 11.2 ± 0.6 %. Zeta potential values for the blank and KGN CH MPs were positive (28.8 ± 3.7 mV and 34.2 ± 0.37 mV, respectively). All results are summarized in Table 1.

When these MPs were visualized by SEM (Fig. 3DE), there was one MP main population with particle size diameters between 2 and 5 μm and another population with diameters between 5 and 20 μm. The micrographs revealed that the MPs were spherical, and the smallest ones presenting a shrunk morphology. The remaining MPs were swollen and sometimes ruptured, especially for blank CH MPs. At higher magnifications, blank CH MPs exhibited smooth surfaces (Fig. 3D). In contrast, the surface of KGN CH MPs (Fig. 3E) was rougher, and some KGN NCs

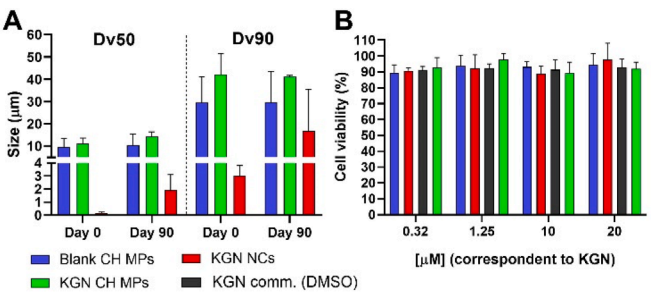

Fig. 4. (A) Fresh (Day 0) *vs.* 90-day stored (2–8 °C) KGN NCs, blank and KGN CH MPs. PSD Dv50 and Dv90 values shown were measured by laser diffraction after resuspension. (B). *In vitro* proliferation activity WST-1 tests. Primary HFLS were incubated for 72 h with a commercial KGN solution (dissolved in 10 % DMSO), KGN NCs, blank and KGN CH MPs. All values are the mean ± sd (n = 3).

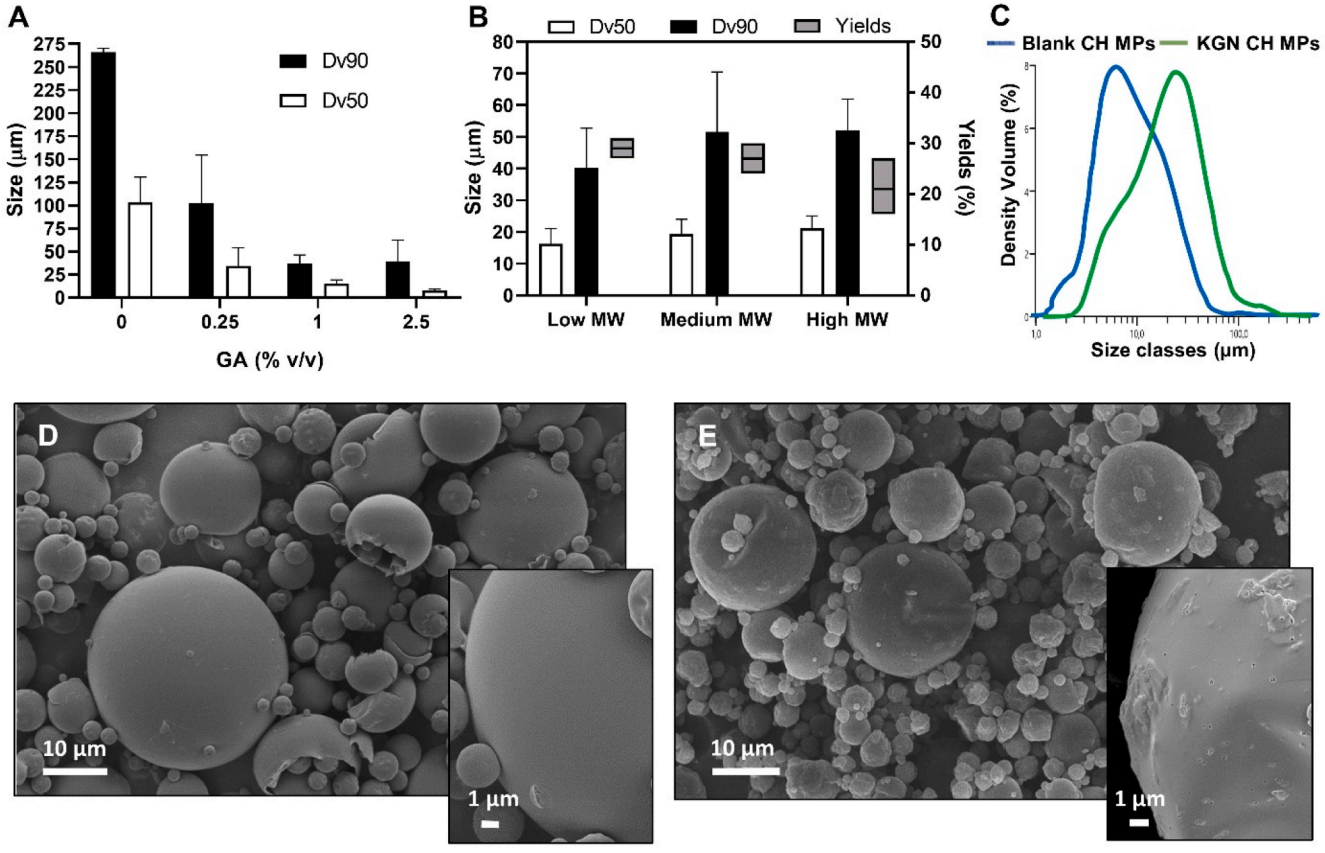

Fig. 3. (A) Crosslinking effect (GA addition) on the PSD Dv50 and Dv90 values of the blank CH MPs (n = 3 different CH MWs). (B) CH MW effect on the PSD (Dv50 Dv90) and yield values. Fixed GA ratio was 1 % v/v. PSD Dv50 and Dv90 values shown were measured by laser diffraction. Yields are expressed as a percentage (100 % is the initial mass weighted). Values are the mean ± s.d. (n = 3). (C) PSD representative graphs by volume density obtained by laser diffraction of blank and KGN CH MPs (GA 1 % v/v and low MW CH). SEM representative micrographs of (D) blank CH MPs and (E) KGN CH MPs at two different magnifications.

Table 1
Final characterization of spray dried formulations.

MPs	Span	D [3:2] (μm)	D [4;3] (μm)	Dv (10) (μm)	Dv (50) (μm)	Dv (90) (μm)	Zp (mV)	EE (%)	DL (% w/w)	Yield (%)*
Blank CH MPs	2.7	7.4	16.7	3.7	9.5	29.6	28.8	–	–	33.3
KGN CH MPs	3.2	9.0	20.6	4.2	11.2	42.3	34.2	70	11.2	33.5

PSD values by density volume were measured by laser diffraction. KGN was quantified by UHPLC. Data show only the mean ($n \geq 3$). Zp, zeta potential; EE, efficacy of encapsulation; DL, drug loading. *100 % is the initial mass (CH + NCs) weighted.

were inserted. Notwithstanding, MPs integrity/sphericity was preserved after NCs incorporation, and KGN-free NCs were not observed.

3.4. Chitosan microspheres presented long-term resuspendability and were nontoxic in vitro

KGN NC and CH MP formulations were stored at 2–8 °C for three months to evaluate variations in PSD over time. As seen in Fig. 4A, PSD Dv50 and Dv90 values for the blank and KGN CH MPs remained similar in comparison with the fresh powder formulations. Dv50 values were increased by 1.1- and 1.27-fold for the blank and KGN CH MPs, respectively, whereas Dv90 values did not vary. However, for the KGN NCs (*i.e.,* an aqueous nanosuspension), Dv50 and Dv90 changes were clearly visible (Fig. 4A, in red), indicating the presence of larger aggregates after three months. Compared to the fresh aqueous nanosuspensions, the Dv50 and Dv90 values were augmented by 10 and 5.6 times, respectively.

In vitro cell proliferation tests were performed on synoviocytes (HFLS) to evaluate the potential toxicity of the formulations in the IA cellular environment. After 72 h, WST-1 results showed that the commercial solution of KGN, KGN NCs, and the correspondent KGN amount of blank and loaded CH MPs did not cause synoviocyte death. Cell proliferation activity remained between 90 and 100 % along the KGN nanomolar and micromolar concentration range, as shown in Fig. 4B. The highest KGN concentration (20 μM) shown in the chart corresponded to an amount of blank or loaded CH MPs around 57.6 μg/mL.

3.5. Chitosan microspheres displayed a suitable intra-articular profile ex vivo

To study particle stability in the IA environment, PSD Dv50 and Dv90 values were measured after incubation in horse SF. Compared with the fresh formulations, results in Fig. 5A show that Dv50 values increased 1.33 and 1.21 times for the blank and KGN CH MPs, respectively. Dv90 values for blank MPs were increased by 1.26-fold but only 1.01 for the KGN CH MPs. KGN NCs PSD variations were not comparable here due to their impactful dissolution in the biologic media. Nonetheless, these results were also plotted (Fig. 5A, in red) given that high Dv90 values were observed in comparison with the fresh formulation (155.5 instead of 3.0 μm). In the same way, particle surface charge changes were also evaluated after the formulations were incubated in SF. The graph in Fig. 5B shows that the native positive zeta potential values of the blank and loaded CH MPs (*i.e.,* 28 and 34 mV, respectively) became slightly negative (−14 and −11 mV). The values for the KGN NCs remained almost unaltered (between −21 and –23 mV). Sample formulations were also recovered and visualized by SEM to reinforce previous data. Some aggregates and/or recrystallization events could be observed in the sample corresponding to the KGN NCs (Fig. 5C). Even though blank and loaded CH MPs (Fig. 5D and E, respectively) exhibited

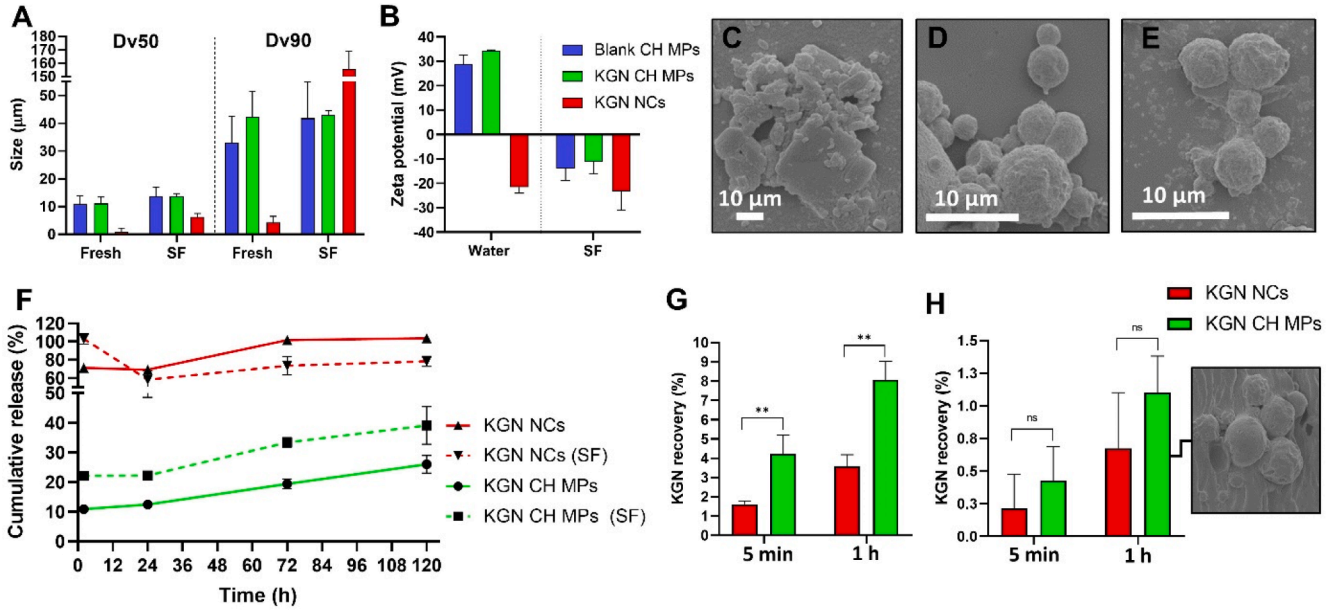

Fig. 5. Fresh (Day 0) *vs.* SF-incubated KGN NCs, blank CH MPs, and KGN CH MPs. (A) PSD Dv50 and Dv90 values were measured by laser diffraction and (B) Zeta potential. SEM representative micrographs of washed KGN NCs (C), blank CH MPs (D), and KGN CH MPs (E) after 1 h incubation in SF. (F) KGN cumulative release in percentage *vs.* time for KGN NCs (red) and KGN CH MPs (green) in PBS (continuous lines) and SF (dotted lines). Release medium was replaced at 24 and 72 h to mimic IA SF clearance. KGN was quantified by UHPLC. KGN bovine cartilage recovery from KGN NCs and KGN CH MPs incubated in (G) PBS and (H) SF. KGN was extracted with ACN from washed cartilage and quantified by UHPLC. A representative SEM micrograph of KGN CH MPs deposited on the cartilage surface after 1 h incubation in SF is also shown. All results are represented by the mean ± sd ($n \geq 3$). * $p < 0.05$, ** $p < 0.01$; ns means. (For interpretation of the references to colour in this figure legend, the reader is referred to the web version of this article.)

a biological surface decoration, sphericity was preserved.

To elucidate the drug release profile of the formulations after a hypothetical IA injection, the drug release setup was designed in saturation conditions (1 mg/mL) and IA SF clearance was reproduced. Fig. 5F depicts the cumulative KGN release from KGN NCs and KGN CH MPs in both PBS and SF over 5 days. In agreement with Section 3.2, KGN concentrations in solution in the biological media (SF) were higher than those in PBS. In the buffer solution, KGN release detected from KGN NCs (Fig. 5F, red continuous line) was approximately 70 % after 24 h, and all content was released/dissolved after 72 h. KGN NCs in the SF media (Fig. 5F, red dotted line) were completely dissolved after 2 h; notably, cumulative release values then decreased to 58 % after 24 h, again increasing to 78 % at 120 h. For KGN CH MPs, a burst release of approximately 11 and 22 % was observed after 2 h in PBS (Fig. 5F, green continuous lines) and SF (Fig. 5F, green dotted lines), respectively. Thereafter, a slower drug release profile was observed until Day 5, reaching approximately 26 and 39 % of the total KGN dose.

In the last section of the study, the capacity of the CH MPs (positively charged) to deliver KGN to cartilage (negatively charged) was investigated. For that, formulations were incubated in an *ex vivo* set up containing a sample of bovine cartilage soaked in PBS or SF. After 1 h in PBS (Fig. 5G), KGN total cartilage recovery from KGN CH MPs represented 8 % of the total dose. Importantly, these values were significantly higher (2.26 times) than the percentage obtained with KGN NCs, which was used as a control. In the SF (Fig. 5H), KGN mean recoveries from KGN CH MPs reached 1.1 % after 1 h over the 0.67 % obtained with its drug nanosuspension counterpart. As seen on the right of Fig. 5H, when cartilage samples were scouted by SEM, some CH MPs were encountered attached on the cartilage surface (for further details see SM, Fig. S5DE).

4. Discussion

Currently, the therapeutic perspectives in OA are contingent upon the discovery of efficacious DMOADs together with the promotion of novel IA drug delivery systems. In the first section of this work, we reported a simple method to synthesize the small molecule DMOAD KGN in one step (Fig. 1A). This reaction was adapted from the chemical route reported by Massaro et al.(Massaro et al., 2019) and Shi et al.(Shi et al., 2016), but acidic reagents were excluded to prevent the importunate sub-formation of the isoindole-1,3-dione derivative shown in Fig. S3. High-shear wet milling was then performed to reduce the size of KGN with the following main objectives: (i) obtaining KGN NCs as a preliminary aqueous nanosuspension. This formulation not only unlocks a possible IA injection of KGN but is also expected to augment its solubility and dissolution rates; (ii) obtaining KGN NCs as a preparatory formulation step prior to spray drying (*i.e.*, to incorporate the NCs into micron-sized CH MPs and improve the IA drug delivery system further).

In agreement with previous reports, the production of NCs by wet milling succeeded after solvent-controlled recrystallization (Fig. 1C); thus, we could “standardize” the homogeneity and quality of the starting material (Maudens et al., 2018b; Salgado et al., 2020). In the same way, only the addition of surfactants/stabilizers leads to PSD values in the nanosize range (Fig. 1DEF), preventing recrystallization/aggregation events (Van Eerdenbrugh et al., 2008). In this study, the biocompatible and nonionic surfactant TPGS at a drug/surfactant ratio of 1/0.1 was selected based on previous experience (Maudens et al., 2018b; Salgado et al., 2020; Sotthivirat et al., 2020). In addition, by adding PVP as another stabilizer control, it was suggested that this actor could be replaced if needed by other excipients used in NC formulation development, such as poloxamers or polysorbates (Ferrar et al., 2020). Solubility tests in Milli-Q water (Fig. 2A) confirmed that KGN, with a LogP of approximately 3.47, is “practically insoluble” (<0.1 mg/mL) according to the Eur. Ph definition, a property that has clearly hindered the clinical translation of KGN to date. For this reason, formulated KGN NCs provide a suitable aqueous nanosuspension that is ready for injection at high KGN concentrations (>10 mg/mL). Moreover, KGN NCs also significantly increased the solubility values observed for recrystallized and commercial KGN, most likely due to their higher specific surface area (Huang et al., 2022). Interestingly, concentrations were considerably increased (0.1–1 mg/mL) for all the samples in physiologically mimicked conditions (*e.g.,* PBS pH 7.2–7.4 at 37 °C), indicating that KGN possesses pH-dependent solubility (the predicted pKa of the weakly acidic KGN is approximately 3.45). It was suggested that these conditions counteracted the solubility-enhancing effect of NCs previously observed in water (pH 6–7) at 20 °C. Nevertheless, in comparison with the native drugs, KGN NCs clearly showed faster dissolution rates in PBS (Fig. 2D). This further supports the potential of these classes of formulations and helps explain their emerging consolidation in the market (Malamatari et al., 2018; Van Eerdenbrugh et al., 2008).

As previously stated, the therapeutic success of drug/DMOAD IA injections also relies on the efficacy of the drug delivery system. This is mainly due to the short retention time and rapid clearance of drugs from the joint, which can be extended to some proteins and nanocarriers (Evans et al., 2014; Maudens et al., 2018a). With this in mind, spray drying was used to upgrade the features of the previous formulation. Similar to a continuous process, the freshly wet milled aqueous nanosuspensions were directly incorporated in the feed aqueous spray drying solution containing a hydrophilic polymer (CH). With this technology approach previously developed in our laboratory for hydrophobic polymers, NCs are loaded in an MP scaffold (Maudens et al., 2018b; Rodríguez-Nogales et al., 2023); additionally, this approach eliminates one intermediate drying step for NCs since organic solvents are not needed. In recent decades, CH has been proposed as a key delivery system for the oral route (Mohammed et al., 2017) but also for IA administration. CH is considered a safe pharmaceutical excipient for the parenteral route, and it is reported to accelerate the wound healing process and exhibit antimicrobial properties (Bellich et al., 2016; Desai et al., 2023; Patrulea et al., 2015). For instance, celecoxib or lornoxicam was encapsulated in CH MPs for IA treatment of arthritis (Abd-Allah et al., 2016; Thakkar et al., 2004). Furthermore, a novel IA carboxymethyl-CH fluid implant was recently reported to be safe and effective for treating symptomatic knee OA in clinical trials (Emans et al., 2023). Most of these researchers implemented classic ionotropic gelation or emulsification techniques but not the pair wet milling + spray drying. The eligibility of these techniques to encapsulate poorly soluble drugs is also debatable. Perhaps for that reason, Kang et al. covalently bound KGN to CH using EDC/NHS catalysis to form afterwards CH NPs and MPs by ionic gelation (Kang et al., 2014). Our approach is simpler because drug loading is driven by a cumulative addition of the drug nanosuspension (KGN NCs) and is not limited by the dissolution capacity of the feed solution.

In this study, CH crosslinking was required, in agreement with many other spray dried and non spray dried CH formulations (He et al., 1999). Based on the spray drying screening reported by Desai et al., chemical crosslinking with GA was selected (Desai and Park, 2005). Here, the aldehyde groups from GA form covalent imine bonds with the amino groups of CH *via* a Schiff reaction. As seen in Fig. 3A, increasing amounts of GA resulted in more homogeneous PSD values and thus an easy resuspension of the MP powder. Without GA, MPs could not be dispersed properly due to MP swelling and rapid dissolution. GA is a widely used cross-linker for this purpose, and was implemented in the clinic for collagen injectable biomaterials (Kershen et al., 2002); however, its potential toxicity limits its use at the present time. This restriction has spurred the search for other alternatives to ensure safe parenteral administration *in vivo*. In the scaling-up process, it must be verified that all GA is bound to CH so that it acts only as an intermediate compound, not being present in the final formulation. Otherwise, our prototype should be reformulated using less toxic cross-linkers, such as genipin (Yu et al., 2021). However, ionic cross-linkers, such as the well-known tripolyphosphate polyanion, were not considered in this work to generate more rigidity and prevent MPs from prematurely swelling (Desai and Park, 2005). Changing the MWs of CH was not impactful even though

low MW CH was preferred for its successful scale-up and parenteral safety. For instance, high MW CH feed solutions were too viscous for the spray drying system, especially for the bi-fluid nozzle. Through these optimizations, reproducible batches of blank and loaded CH MPs were formulated at the laboratory scale (yields > 30–40 %) with encapsulation efficacies of approximately 70 % (Table 1). Laser diffraction graphs and SEM images of the final formulations showed that the particle size ranged between approximately 2 and 40 μm with no apparent particle agglomerates (Table 1 and Fig. 3). This result also represents an outstanding MP resuspension performance for lab-scale production while maintaining a particle size compatible with safe IA injection and enabling a delay in clearance from the joint space (Pradal et al., 2016). In addition, powder resuspendability was barely affected by hygroscopic growth or particle clustering after 3 months of storage. Concerning preliminary long-term storage, this result highlights that KGN CH MPs exhibit an additional formulation asset over aqueous nanosuspensions (KGN NCs), which are more prone to aggregate and/or recrystallize over time, as observed in Fig. 4A.

In the last section of this work, we shed light on the performance of KGN CH MPs in the IA environment after a simulated administration. For that, their preliminary toxicity *in vitro* profile was evaluated on HFLS as these cells are nearest to the formulation after an IA injection. Over the equivalent KGN concentration range (up to 20 μM) in Fig. 4B, blank or loaded MPs did not impair the cell proliferation activity of these knee synoviocytes at reported therapeutic concentrations. For instance, 10 μM KGN promoted cartilage repair in surgery-induced OA model mice (Johnson et al., 2012). Then, MP incubation in IA biologic medium (*i.e.,* horse SF at 37 °C) did not trigger substantial particle growth, instability or aggregation (Fig. 5A). Even though particle swelling is always expected with CH, the moderate Dv50 and Dv90 increments shown were attributed to the rigidity provided by GA crosslinking. Under the same conditions, the positive surface charge of CH MPs was neutralized or negativized (Fig. 5B). This revealed an interaction with the proteins and other compounds, such as hyaluronic acid (negatively charged), present in the SF. This biological MP coating, well acknowledged as soft or hard protein/biomolecular corona, could be visualized by SEM (Fig. 5DE), and it is reported to induce this surface charge inversion (Marques et al., 2023; Tenzer et al., 2013). Although this event did not entail noticeable MP morphology changes or aggregation, it could explain the differences found in cartilage retention between PBS and SF. Here, the cationic nature of the CH MPs was hypothesized to increase their anchorage to the negatively charged cartilage surface (where KGN exerts its main action) (Hou et al., 2021). This targeting strategy has been reported for many positively charged drug delivery systems in which their cationic domains interact electrostatically with glycosaminoglycans containing negatively charged chondroitin and keratan sulfate moieties (Bajpayee and Grodzinsky, 2017; Vedadghavami et al., 2019). Through the *ex vivo* cartilage setup, we could observe that CH MPs significantly increased KGN retention on cartilage in PBS compared with the KGN NCs (Fig. 5G). As shown in Fig. S6AB, we previously observed similar outcomes in a pilot *in vitro* study using a type “A” gelatin surface. In the presence of SF, we observed a similar trend, but KGN retention on cartilage dropped considerably (Fig. 5H), corresponding with the studies of von Mentzer et al., with cationic polyamidoamine dendrimers (von Mentzer et al., 2022). This highlights the importance of performing *ex vivo* experiments using biological fluids, such as the ones accomplished in this work. These are rarely seen in the literature but consider protein or biomolecular corona formation on the drug delivery system.

By working again in parallel with PBS and SF, it was confirmed that the formulations also behaved slightly different in the IA drug release study shown in Fig. 5F. In SF, MPs exhibited a moderate burst release and then a controlled release profile, whereas the NCs released all their content from the beginning of the experiment. The higher solubility of KGN in SF previously shown in Fig. 2C led to the precipitation/recrystallization of KGN NCs in saturation conditions after 24 h. KGN CH MPs, which could release their content in “sink” conditions over 24 h (Fig. S6C), exhibited a cumulative drug release responsive to the mimicked IA fluid clearance (as occurs in the IA compartment) (Owen et al., 1994). Here, the protonated amino groups of CH MPs create a slightly acidic microenvironment that can limit the pH solubility of KGN and therefore modulate its release from the MPs. The pH of the OA knee oscillates from 7.25 to 7.8 and from 6.0 to 7.40 for rheumatic joint diseases, approximately (Goldie and Nachemson, 1970; Milošev et al., 2017; Wen et al., 2023). The pH measured in our release medium (6.47 ± 0.03) remained above the favorable limits for parenteral formulations (Roethlisberger et al., 2017). The “sink” conditions of the IA compartment may remain questionable, but we should expect a higher IA buffering capacity *in vivo*, which might be translated into faster KGN release (*e.g.,* 3–5 days).

5. Conclusion

The poor therapeutic outlook of OA continues to inspire a persistent search for efficient IA treatments. We have presented a combined technological approach (wet milling + spray drying) to develop an IA formulation consisting of CH MPs loaded with DMOAD KGN NCs. This batch-driven but practically continuous process is easy, fast, cost-effective, and therefore portrays a suitable scale-up scenario. Positively charged KGN CH MPs can be stored as a ready-to-use powder, displaying a particle size compatible with IA administration (2–40 μm) after resuspension. By working in parallel in PBS and SF, we could better understand the performance of this formulation in a simulated IA environment. Here, the formulation was nontoxic in human synoviocytes *in vitro* and remained stable in the IA biologic fluid. The CH MPs also exhibited KGN controlled release and prevented premature NC recrystallization. However, their cartilage adhesion/retention abilities encountered *ex vivo* remain more questionable, probably due to biomolecule corona formation. Further preclinical investigations in OA animal models will shed light on the therapeutic potential of this approach. It is also important to emphasize that this technology platform can be exploited for other administration routes (*e.g.,* oral or topical), entailing the delivery of poorly soluble drugs.

CRediT authorship contribution statement

Luca Morici: Writing – original draft, Methodology, Investigation, Formal analysis, Data curation. **Paula Gonzalez-Fernandez:** Writing – original draft, Validation, Resources, Investigation. **Sébastien Jenni:** Methodology, Investigation, Formal analysis. **Alexandre Porcello:** Validation, Resources, Methodology. **Eric Allémann:** Writing – review & editing, Validation, Supervision, Resources. **Olivier Jordan:** Writing – review & editing, Validation, Supervision, Conceptualization. **Carlos Rodríguez-Nogales:** Writing – review & editing, Validation, Supervision, Methodology, Investigation, Conceptualization.

Declaration of competing interest

The authors declare the following financial interests/personal relationships which may be considered as potential competing interests: Paula Gonzalez-Fernandez financial support was provided by Swiss National Science Foundation (SNSF), project 205321_184936. If there are other authors, they declare that they have no known competing financial interests or personal relationships that could have appeared to influence the work reported in this paper.

Data availability

Data will be made available on request.

Acknowledgments

We thank the financial support provided by the Swiss National

Science Foundation (SNSF) project 205321_184936. The authors would like also to thank Ms. Nathalie Boulens and Ms. Justine Langham for their technical support in acquiring the SEM micrographs and UHPLC quantifications, respectively.

Appendix A. Supplementary data

Supplementary data to this article can be found online at https://doi.org/10.1016/j.ijpharm.2023.123754.

References

Abd-Allah, H., Kamel, A.O., Sammour, O.A., 2016. Injectable long acting chitosan/tripolyphosphate microspheres for the intra-articular delivery of lornoxicam: Optimization and in vivo evaluation. Carbohydr. Polym. 149, 263–273. https://doi.org/10.1016/J.CARBPOL.2016.04.096.

Aranaz, I., Alcántara, A.R., Civera, M.C., Arias, C., Elorza, B., Caballero, A.H., Acosta, N., 2021. Chitosan: An Overview of Its Properties and Applications. Polymers (basel) 13. https://doi.org/10.3390/POLYM13193256.

Bajpayee, A.G., Grodzinsky, A.J., 2017. Cartilage-targeting drug delivery: can electrostatic interactions help? Nat. Rev. Rheumatol. 13, 183–193. https://doi.org/10.1038/NRRHEUM.2016.210.

Bellich, B., D'Agostino, I., Semeraro, S., Gamini, A., Cesàro, A., 2016. "The Good, the Bad and the Ugly" of Chitosans. Mar. Drugs 14. https://doi.org/10.3390/MD14050099.

Chen, P., Liao, X., 2023. Kartogenin delivery systems for biomedical therapeutics and regenerative medicine. Drug Deliv. 30, 2254519. https://doi.org/10.1080/10717544.2023.2254519.

Desai, N., Rana, D., Salave, S., Gupta, R., Patel, P., Karunakaran, B., Sharma, A., Giri, J., Benival, D., Kommineni, N., 2023. Chitosan: A Potential Biopolymer in Drug Delivery and Biomedical Applications. Pharmaceutics 2023, Vol. 15, Page 1313 15, 1313. 10.3390/PHARMACEUTICS15041313.

Desai, K.G.H., Park, H.J., 2005. Preparation of cross-linked chitosan microspheres by spray drying: effect of cross-linking agent on the properties of spray dried microspheres. J. Microencapsul. 22, 377–395. https://doi.org/10.1080/02652040500100139.

Emans, P.J., Skaliczki, G., Haverkamp, D., Bentin, J., Chausson, M., Schifflers, M., Portelange, N., 2023. KiOmedine® CM-Chitosan is Effective for Treating Advanced Symptomatic Knee Osteoarthritis up to Six Months Following a Single Intra-Articular Injection: A Post Hoc Analysis of Aproove Clinical Study. Open Rheumatol J 17. https://doi.org/10.2174/18743129-V16-E220206-2022-19.

Evans, C.H., Kraus, V.B., Setton, L.A., 2014. Progress in intra-articular therapy. Nat. Rev. Rheumatol. 10, 11. https://doi.org/10.1038/NRRHEUM.2013.159.

Ferrar, J.A., Sellers, B.D., Chan, C., Leung, D.H., 2020. Towards an improved understanding of drug excipient interactions to enable rapid optimization of nanosuspension formulations. Int. J. Pharm. 578 https://doi.org/10.1016/J.IJPHARM.2020.119094.

Goldie, I., Nachemson, A., 1970. Synovial pH in rheumatoid knee joints. II. The effect of local corticosteroid treatment. Acta Orthop. Scand. 41, 354–362. https://doi.org/10.3109/17453677008991521.

Gonzalez-Fernandez, P., Rodríguez-Nogales, C., Jordan, O., Allémann, E., 2022. Combination of mesenchymal stem cells and bioactive molecules in hydrogels for osteoarthritis treatment. Eur. J. Pharm. Biopharm. 172, 41–52. https://doi.org/10.1016/J.EJPB.2022.01.003.

He, P., Davis, S.S., Illum, L., 1999. Chitosan microspheres prepared by spray drying. Int. J. Pharm. 187, 53–65. https://doi.org/10.1016/S0378-5173(99)00125-8.

Hou, M., Zhang, Y., Zhou, X., Liu, T., Yang, H., Chen, X., He, F., Zhu, X., 2021. Kartogenin prevents cartilage degradation and alleviates osteoarthritis progression in mice via the miR-146a/NRF2 axis. Cell Death & Disease 2021 12:5 12, 1–16. 10.1038/s41419-021-03765-x.

Huang, Z., Staufenbiel, S., Bodmeier, R., 2022. Combination of co-crystal and nanocrystal techniques to improve the solubility and dissolution rate of poorly soluble drugs. Pharm. Res. 39, 949–961. https://doi.org/10.1007/S11095-022-03243-9.

Johnson, K., Zhu, S., Tremblay, M.S., Payette, J.N., Wang, J., Bouchez, L.C., Meeusen, S., Althage, A., Cho, C.Y., Wu, X., Schultz, P.G., 2012. A stem cell-based approach to cartilage repair. Science 336, 717–721. https://doi.org/10.1126/SCIENCE.1215157.

Kang, M.L., Ko, J.Y., Kim, J.E., Im, G.I., 2014. Intra-articular delivery of kartogenin-conjugated chitosan nano/microparticles for cartilage regeneration. Biomaterials 35, 9984–9994. https://doi.org/10.1016/J.BIOMATERIALS.2014.08.042.

Kantak, M.N., Bharate, S.S., 2022. Analysis of clinical trials on biomaterial and therapeutic applications of chitosan: A review. Carbohydr. Polym. 278, 118999 https://doi.org/10.1016/J.CARBPOL.2021.118999.

Kershen, R.T., Dmochowski, R.R., Appell, R.A., 2002. Beyond collagen: injectable therapies for the treatment of female stress urinary incontinence in the new millennium. Urol. Clin. North Am. 29, 559–574. https://doi.org/10.1016/S0094-0143(02)00066-6.

Leifer, V.P., Katz, J.N., Losina, E., 2022. The burden of OA-health services and economics. Osteoarthritis Cartilage 30, 10–16. https://doi.org/10.1016/J.JOCA.2021.05.007.

Malamatari, M., Taylor, K.M.G., Malamataris, S., Douroumis, D., Kachrimanis, K., 2018. Pharmaceutical nanocrystals: production by wet milling and applications. Drug Discov. Today 23, 534–547. https://doi.org/10.1016/J.DRUDIS.2018.01.016.

Marini, J.C., Forlino, A., Matrix Branch, E., Kennedy Shriver, E., 2012. Replenishing Cartilage from Endogenous Stem Cells HHS Public Access. N. Engl. J. Med. 366, 2522–2524. https://doi.org/10.1056/NEJMcibr1204283.

Marques, C., Hajipour, M.J., Marets, C., Oudot, A., Safavi-sohi, R., Guillemin, M., Borchard, G., Jordan, O., Saviot, L., Maurizi, L., 2023. Identification of the Proteins Determining the Blood Circulation Time of Nanoparticles. ACS Nano 17. https://doi.org/10.1021/ACSNANO.3C02041.

Massaro, M., Buscemi, G., Arista, L., Biddeci, G., Cavallaro, G., D'Anna, F., Di Blasi, F., Ferrante, A., Lazzara, G., Rizzo, C., Spinelli, G., Ullrich, T., Riela, S., 2019. Multifunctional Carrier Based on Halloysite/Laponite Hybrid Hydrogel for Kartogenin Delivery. ACS Med. Chem. Lett. 10, 419–424. https://doi.org/10.1021/ACSMEDCHEMLETT.8B00465/SUPPL_FILE/ML8B00465_SI_001.PDF.

Maudens, P., Jordan, O., Allémann, E., 2018a. Recent advances in intra-articular drug delivery systems for osteoarthritis therapy. Drug Discov. Today 23, 1761–1775. https://doi.org/10.1016/J.DRUDIS.2018.05.023.

Maudens, P., Seemayer, C.A., Thauvin, C., Gabay, C., Jordan, O., Allémann, E., 2018b. Nanocrystal-Polymer Particles: Extended Delivery Carriers for Osteoarthritis Treatment. Small 14. https://doi.org/10.1002/SMLL.201703108.

Milošev, I., Levašič, V., Vidmar, J., Kovač, S., Trebše, R., 2017. pH and metal concentration of synovial fluid of osteoarthritic joints and joints with metal replacements. J. Biomed. Mater. Res. B Appl. Biomater. 105, 2507–2515. https://doi.org/10.1002/JBM.B.33793.

Mohammed, M.A., Syeda, J.T.M., Wasan, K.M., Wasan, E.K., 2017. An Overview of Chitosan Nanoparticles and Its Application in Non-Parenteral Drug Delivery. Pharmaceutics 9. https://doi.org/10.3390/PHARMACEUTICS9040053.

Owen, S., Francis, H., Roberts, M., 1994. Disappearance kinetics of solutes from synovial fluid after intra-articular injection. Br. J. Clin. Pharmacol. 38, 349. https://doi.org/10.1111/J.1365-2125.1994.TB04365.X.

Paik, J., Duggan, S.T., Keam, S.J., 2019. Triamcinolone Acetonide Extended-Release: A Review in Osteoarthritis Pain of the Knee. Drugs 79, 455. https://doi.org/10.1007/S40265-019-01083-3.

Patrulea, V., Ostafe, V., Borchard, G., Jordan, O., 2015. Chitosan as a starting material for wound healing applications. Eur. J. Pharm. Biopharm. 97, 417–426. https://doi.org/10.1016/J.EJPB.2015.08.004.

Pradal, J., Maudens, P., Gabay, C., Seemayer, C.A., Jordan, O., Allémann, E., 2016. Effect of particle size on the biodistribution of nano- and microparticles following intra-articular injection in mice. Int. J. Pharm. 498, 119–129. https://doi.org/10.1016/J.IJPHARM.2015.12.015.

Rodríguez-Nogales, C., Meeus, J., Thonus, G., Corveleyn, S., Allémann, E., Jordan, O., 2023. Spray-dried nanocrystal-loaded polymer microparticles for long-term release local therapies: an opportunity for poorly soluble drugs. Drug Deliv. 30, 2284683. https://doi.org/10.1080/10717544.2023.2284683.

Roethlisberger, D., Mahler, H.C., Altenburger, U., Pappenberger, A., 2017. If Euhydric and Isotonic Do Not Work, What Are Acceptable pH and Osmolality for Parenteral Drug Dosage Forms? J. Pharm. Sci. 106, 446–456. https://doi.org/10.1016/J.XPHS.2016.09.034.

Salgado, C., Guénée, L., Černý, R., Allémann, E., Jordan, O., 2020. Nano wet milled celecoxib extended release microparticles for local management of chronic inflammation. Int. J. Pharm. 589 https://doi.org/10.1016/J.IJPHARM.2020.119783.

Shi, D., Xu, X., Ye, Y., Song, K., Cheng, Y., Di, J., Hu, Q., Li, J., Ju, H., Jiang, Q., Gu, Z., 2016. Photo-cross-linked scaffold with kartogenin-encapsulated nanoparticles for cartilage regeneration. ACS Nano 10, 1292–1299. https://doi.org/10.1021/ACSNANO.5B06663/SUPPL_FILE/NN5B06663_SI_001.PDF.

Sosnik, A., Seremeta, K.P., 2015. Advantages and challenges of the spray-drying technology for the production of pure drug particles and drug-loaded polymeric carriers. Adv. Colloid Interface Sci. 223, 40–54. https://doi.org/10.1016/J.CIS.2015.05.003.

Sotthivirat, S., Ramesh, R., Wasylaschuk, W., Bottone, C., Xia, B., Stellabott, J., McNevin, M., Skomski, D., Brown, C., 2020. Effect of TPGS surfactant on dissolution sensitivity of a poorly water-soluble drug using high-shear wet granulation. Powder Technol. 375, 302–309. https://doi.org/10.1016/J.POWTEC.2020.07.093.

Tenzer, S., Docter, D., Kuharev, J., Musyanovych, A., Fetz, V., Hecht, R., Schlenk, F., Fischer, D., Kiouptsi, K., Reinhardt, C., Landfester, K., Schild, H., Maskos, M., Knauer, S.K., Stauber, R.H., 2013. Rapid formation of plasma protein corona critically affects nanoparticle pathophysiology. Nat. Nanotechnol. 8, 772–781. https://doi.org/10.1038/NNANO.2013.181.

Thakkar, H., Sharma, R.K., Mishra, A.K., Chuttani, K., Murthy, R.S.R., 2004. Celecoxib incorporated chitosan microspheres: in vitro and in vivo evaluation. J. Drug Target. 12, 549–557. https://doi.org/10.1080/10611860400010630.

Van Eerdenbrugh, B., Van den Mooter, G., Augustijns, P., 2008. Top-down production of drug nanocrystals: Nanosuspension stabilization, miniaturization and transformation into solid products. Int. J. Pharm. 364, 64–75. https://doi.org/10.1016/J.IJPHARM.2008.07.023.

Vårum, K.M., Ottøy, M.H., Smidsrød, O., 1994. Water-solubility of partially N-acetylated chitosans as a function of pH: effect of chemical composition and depolymerisation. Carbohydr. Polym. 25, 65–70. https://doi.org/10.1016/0144-8617(94)90140-6.

Vedadghavami, A., Wagner, E.K., Mehta, S., He, T., Zhang, C., Bajpayee, A.G., 2019. Cartilage Penetrating Cationic Peptide Carriers for Applications in Drug Delivery to Avascular Negatively Charged Tissues. Acta Biomater. 93, 258. https://doi.org/10.1016/J.ACTBIO.2018.12.004.

von Mentzer, U., Selldén, T., Råberg, L., Erensoy, G., Hultgård Ekwall, A.K., Stubelius, A., 2022. Synovial fluid profile dictates nanoparticle uptake into cartilage - implications of the protein corona for novel arthritis treatments. Osteoarthritis Cartilage 30, 1356–1364. https://doi.org/10.1016/J.JOCA.2022.07.002.

Warren, M.R., Vedadghavami, A., Bhagavatula, S., Bajpayee, A.G., 2022. Effects of polycationic drug carriers on the electromechanical and swelling properties of cartilage. Biophys. J . 121 https://doi.org/10.1016/J.BPJ.2022.06.024.

Wen, J., Li, H., Dai, H., Hua, S., Long, X., Li, H., Ivanovski, S., Xu, C., 2023. Intra-articular nanoparticles based therapies for osteoarthritis and rheumatoid arthritis management. Mater Today Bio 19, 100597. https://doi.org/10.1016/J.MTBIO.2023.100597.

Yu, Y., Xu, S., Li, S., Pan, H., 2021. Genipin-cross-linked hydrogels based on biomaterials for drug delivery: a review. Biomater. Sci. 9, 1583–1597. https://doi.org/10.1039/D0BM01403F.

Ziaee, A., Albadarin, A.B., Padrela, L., Femmer, T., O'reilly, E., Walker, G., 2018. Spray drying of pharmaceuticals and biopharmaceuticals: Critical parameters and experimental process optimization approaches. 10.1016/j.ejps.2018.10.026.